Saudi Journal of Biological Sciences (2017) **24**, 495–503

King Saud University

Saudi Journal of Biological Sciences

www.ksu.edu.sa
www.sciencedirect.com

ORIGINAL ARTICLE

Angiotensin II-accelerated vulnerability of carotid plaque in a cholesterol-fed rabbit model-assessed with magnetic resonance imaging comparing to histopathology

Beibei Sun [a], Huilin Zhao [a,*], Xiao Li [a], Hong Yao [b], Xiaosheng Liu [a], Qing Lu [a], Jieqing Wan [b], Jianrong Xu [a,*]

[a] *Department of Radiology, Renji Hospital, School of Medicine, Shanghai Jiaotong University, Shanghai 200127, China*
[b] *Department of Neurosurgery, Renji Hospital, School of Medicine, Shanghai Jiaotong University, Shanghai 200127, China*

Received 3 November 2016; revised 28 December 2016; accepted 6 January 2017
Available online 27 January 2017

KEYWORDS

Angiotensin II;
Rabbit model;
Vulnerability;
Magnetic resonance imaging;
Carotid artery

Abstract This study sought to reveal the effect of angiotensin II (Ang II)-induced atherosclerotic vulnerability in rabbits and to determine whether *in vivo* magnetic resonance imaging (MRI) can determine the effect of Ang II on atherosclerotic development over time. In total, 24 elderly male New Zealand white rabbits underwent an intravascular balloon injury in the left common carotid artery (LCCA) and were subsequently fed a high cholesterol diet for 12 weeks. At 8 weeks, rabbits were randomly assigned to receive either Ang II (1.4 mg/kg/d, Ang II group) or vehicle (phosphate-buffered saline, control) via a subcutaneous osmotic minipump for 4 weeks. The rabbits were imaged three times: at baseline and at 8 and 12 weeks. After the 12-week MRI scanning, rabbits were euthanized to obtain pathological and histological data. Atherosclerotic plaques were identified in the 21 rabbits that survived the 12-week trial. Typical feature of vulnerable plaques (VP), intraplaque hemorrhage, were observed in 6 of 10 animals (60.0%) in the Ang II group. The Cohen *K* value of MR imaging between the AHA classifications was 0.82 (0.73–0.91; $P < 0.001$). MRI revealed that the change in carotid morphology were significantly different between the Ang II and control group plaques. Our results support an important role for Ang II in plaque vulnerability by promoting intraplaque neovascularization and hemorrhage as well as inflammation. The vulnerable features induced by Ang II in rabbit carotid plaques could be accurately monitored with MRI *in vivo* and confirmed with histomorphology.

* Corresponding authors.
E-mail addresses: huilinzhao2013@163.com (H. Zhao), renjixjr@163.com (J. Xu).
Peer review under responsibility of King Saud University.

Production and hosting by Elsevier

http://dx.doi.org/10.1016/j.sjbs.2017.01.017

1. Introduction

Carotid vulnerable plaques (VP) may result in rapid worsening of stenosis and thrombus formation leading to stroke in patients with carotid atherosclerosis. Therefore, early detection of VP to allow early and effective interventions has become a major research interest. Pathologically, a typical VP often contains intraplaque hemorrhage (IPH) and a large lipid-rich necrotic core (LRNC) covered by a thin fibrous cap and is infiltrated by inflammatory cells, such as macrophages.

In recent years, a VP of the aorta can be successfully established through a balloon-induced vascular endothelium injury or by transfecting the abdominal aorta with the p53 gene followed by pharmacological triggering in rabbits given a high-fat diet (Qi et al., 2015; Phinikaridou et al., 2010). These types of models have been the most common models used for magnetic resonance imaging (MRI) studies, but few studies have been related to the rabbit carotid model, which is anatomically suitable for further investigation of the stroke caused by carotid atherosclerosis. In addition, some studies aimed at creating a carotid VP model, such as a high cholesterol diet combined with a balloon injury or cast placement, are both unable to create a human-like vulnerable plaque in a limited period (Ma et al., 2008; Den Dekker et al., 2014) because hepatic failure may develop in New Zealand white (NZW) rabbits after the long period of high cholesterol diet. So creating an accelerated VP plaque model in the carotid artery is our major research interest.

Angiotensin II (Ang II) is involved in various vascular events, such as endothelial activation and dysfunction (Pueyo et al., 2000; Laursen et al., 1997), cell proliferation (Kohno et al., 2000) as well as proinflammatory effects (Mervaala et al., 1999) of atherosclerotic lesions. Daiana et al. found that Ang II–induced hypertension can specifically increase the development of atherosclerosis in apoE knockout mice. Others have also reported that the carotid atherosclerotic lesions from Ang II–treated mice display a more pronounced vulnerable plaque phenotype, such as intralesional neovasculature and hemorrhage (Da Cunha et al., 2006; Cheng et al., 2006; Du et al., 2016). Based on these murine models, this study is aimed (1) to test whether Ang II act as an accelerating factor of the lesion by promoting plaque vulnerability in a rabbit atherosclerotic model and (2) to apply MRI measurements to monitor the effect of Ang II on atherosclerotic development over time and to see whether MRI is a useful modality for accurate assessment and follow-up evaluation of plaques.

2. Materials and methods

2.1. Animal model

This experimental protocol was approved by our institutional committee for animal use and care. In total, 24 male elderly NZW rabbits(Department of Laboratory Animal Science of Fudan University, Shanghai) weighing 3.0–3.5 kg were recruited and were fed an atherogenic diet containing 1% cholesterol (120–140 g/day) for 1 week and then subjected to a balloon-induced intimal injury of the left common carotid artery (LCCA). A balloon catheter with diameter of 2.5 mm and a length of 20 mm (Medtronic, AVE, Santa Rosa, CA) was inserted into the LCCA and inflated and deflated three times for 180 s after rabbits had been anesthetized with an intravenous injection of pentobarbital. After balloon injury of the LCCA, rabbits were maintained on a high cholesterol diet until sacrifice at the end of 12 weeks. Four weeks before the end of the trial, animals were randomly assigned to receive subcutaneous implantation of a minipump filled with either angiotensin II (1.44 mg/kg/d, AngII group) or phosphate-buffered saline (control). We choose an infusion rate of angiotensin II previously shown to accelerate atherosclerosis in apoE-KO mice (Daugherty et al., 2000).

2.2. Blood pressure and lipid determination

After anesthetization through the auricular vein but prior to sacrifice, catheters were placed in the right femoral artery for recording of the rabbit's arterial blood pressure. Arterial pressure was measured in a conscious rabbit using a pressure transducer and recorded on a thermal array recorder (RTA 1200 M; Nihon Kohden, Tokyo, Japan). Blood samples were collected from the ear artery at 0 week and the end of the 8-week cholesterol diet prior to the animal being sacrificed. Plasma total cholesterol (TC), triglyceride (TG), high density lipoprotein-cholesterol (HDL-C) and low density lipoprotein-cholesterol (LDL-C) were measured with enzymatic reaction kits from BioVision (Mountain View, Calif) and Wako Chemicals Co (Richmond, VA), respectively.

2.3. Histopathological analysis

Immediately after sacrifice, the injured LCCA tissues were removed from the rabbit and washed in saline. The distances from the surgical cut and the carotid bifurcation were used as internal reference points to co-localize between the MRI findings and the histological specimen. The carotid arteries were marked with suture ligatures on the left bifurcation over the total length imaged by MRI. The specimens were fixed in 10% formalin, sectioned in 3.0-mm transverse slices, decalcified, and embedded in paraffin. The paraffin-embedded specimens were sectioned at 10 μm thickness, stained with hematoxylin and eosin (HE), and subjected to histopathological and immunohistochemical analyses. HE staining was used for routine histopathological examination and compared with the MRI. Atherosclerosis formation was histomorphologically evaluated according to the AHA classifications (Stary et al., 1995).

2.4. Immunohistochemical (IHC) staining

All of the tissue samples were pre-treated as previously described (Torzewski et al., 1998). For Pentraxin3 (PTX3), RAM11 and CD31 staining, slides were first incubated with one of the following primary antibodies: PTX3 (1:200, code LS-B6679, Life span), RAM11 (1:100, code M0633, Dako), CD31 (1:200, code ab9498, Abcam) at 4 °C overnight. After a wash in PBS, sections were incubated with biotinylated anti-mouse secondary antibody (MaiXin Bio, Fuzhou, China) at room temperature for 30 min and then with the avidin–biotinylated horseradish peroxidase complex (ABC Elite kit, Vector, Burlingame, CA, USA) for 30 min. Peroxidase labeling was visualized using 0.2% (v/v) 3, 39-diaminobenzidine as a chromogen. When using the antibodies, the sections were

lightly counterstained with hematoxylin. All of the sections were observed and photographed with an Axioskop 2 microscope (Carl Zeiss, Oberkochen, Germany). PTX3 and RAM11 expression levels were interpreted based on the ratio and intensity of positive-staining cells: $<5\%$ scored 0; 5–24% scored 1; 25–49% scored 2; 50–74% scored 3; and $>74\%$ scored 4 (Zhang et al., 2015). These scores were determined independently by two senior pathologists. $CD31^+$ neovessels in the plaque were counted by light microscopy. Six high-power fields (40×) were acquired for each slice, and the numbers of positively-stained cells in the intima and media were counted. The count was acquired six times and then averaged (Mao et al., 2010).

2.5. High-resolution multi-sequence MR imaging

Serial MRI examinations were performed 3 times, at baseline and at 8 and 12 weeks on a 3.0 T MRI scanner (Achieva; Philips Healthcare, Best, Netherlands) with an 8-channel phased-array carotid coil (Chenguang Medical Technologies, Shanghai, China). Rabbits were sedated with an intravenous injection of 40 mg/kg pentobarbital (Shanghai Chemical Reagent Co., Shanghai), allowing spontaneous respiration throughout the examination. MRI were performed with the rabbits placed in a prone position. A standardized imaging protocol was performed to obtain multi-contrast cross-sectional MRI scans: 3D TOF (TR/TE, 20/4.9 ms; flip angle, 20°), quadruple inversion recovery T1-weighted sequence (TR/TE, 800/10 ms), T2-weighted sequence with multi-double inversion recovery 18 (TR/TE, 4800/50 ms), and 3D MPRAGE sequence (TR/TE, 8.8/5.3 ms, flip angle, 15°). All MRI axial scans were acquired with a section thickness of 3 mm, an FOV of 140 × 90 mm, and a matrix size of 336 × 336. Fat saturation was applied to the acquisition of the black-blood sequences to enhance the tissue contrast between the carotid vessel wall and the surrounding tissues.

2.6. MR imaging analysis

The MR findings were interpreted independently by three radiologists (ZHL, SBB, and HPP) who were experienced with vascular imaging but blinded to the histological findings. Quantitative MRI analyses were also performed by them by consensus. The wall thickness of the injured LCCA or the distance between the outer and inner borders of the cross-section on the carotid artery was measured using commercial software (Vessel Mass, Netherlands). The measurements were usually made on the T1W images, with the T2W images, 3D-TOF and MP-RAGE cross-referenced. The morphological measurements, including the vessel wall area (VWA) and max wall thickness (max WT), were measured for 6 slices of each artery. The presence or absence and the area of each carotid plaque component (e.g., LRNC and IPH, calcification [CA]) in each slice were identified based on a previous study (Saam et al., 2005; Zhao et al., 2013). According to the modified American Heart Association (AHA) criteria (Cai et al., 2002), type I and II = nearly normal vessel wall thickness; type III = diffuse intimal thickening or a small eccentric plaque with no calcification; Type IV–V = plaques characterized by a lipid or necrotic core surrounded by fibrous tissue with possible calcification. Type VI = complex plaque with a possible surface defect, hemorrhage, or thrombus.

2.7. Statistics

All obtained quantitative data were expressed as mean ± standard deviation (SD). Statistical analyses were performed with the SPSS software (SPSS for Windows, version 11.0, 2001; SPSS, Chicago, IL). Cohen's κ coefficient was used to assess agreement between the MRI findings and the histological analysis. *Kappa* ranges from −1 (perfect disagreement) to +1 (perfect agreement), and $kappa \geqslant 0.75$ was defined as strong agreement, $0.4 < kappa < 0.75$ was defined as moderate agreement and $kappa \leqslant 0.4$ was defined as poor agreement (Curvo-Semedo et al., 2011), $P < 0.05$ were considered statistically significant. The effect sizes of plaque parameters to detect plaque development were calculated as the ratio of the mean difference between 8 weeks and follow-up measurements divided by the pooled standard deviation. Effect sizes were compared using a paired *t*-test (Den Hartog et al., 2013). The continuous variables were compared via an independent-samples *t*-test when normally distributed or the Mann–Whitney *U* test when non-normally distributed.

3. Results

Of the 24 rabbits initially selected, 2 from the Ang II group died at 9 weeks due to a suspected multi-organ dysfunction. In the control group, 1 died from an anesthesia accident at 8 weeks.

3.1. Artery pressure and serum lipid assay

At the end of week 12, lipid disorders were led by a high-cholesterol diet, including significantly increased TC, TG, HDL-C and LDL-C compared with the baseline levels ($P < 0.01$) (Fig. 1). In addition, the body weights of the rabbits in the two groups gradually increased over time ($P < 0.05$). However, all these parameters showed no significant difference between the two groups ($P > 0.05$). At 12 weeks, the rabbits' mean systolic pressure in the Ang II group was higher than that in control group rabbits (175.8 ± 7.5 vs 120.8 ± 6.4 mmHg).

3.2. Accelerated effect of Ang II in rabbit carotid atherosclerosis model

Histologically, the 21 rabbits that survived until the end of the study period all had formed various degrees of atherosclerotic plaques. Six rabbits in the Ang II group (6/10, 60.0%) developed VPs (containing IPH) in the LCCA, but no IPH was observed in the control group. Ang II had a dramatic effect on the development of atherosclerosis in the carotid artery. Representative examples of the LCCA after 4 weeks of Ang II and vehicle treatment in the Ang II and control groups are shown in Fig. 2. Note that other than more prominent neointima augmentation and decreased lumen diameter, intimal changes including irregularly developed intralesional neovasculature and hemorrhages were more evident in the Ang II–treated rabbits compared with the control group (Fig. 2).

Additionally, intimal lesions were characterized by the presence of RAM 11-positive macrophage foam cells in both groups, but the most intense staining occurred in the

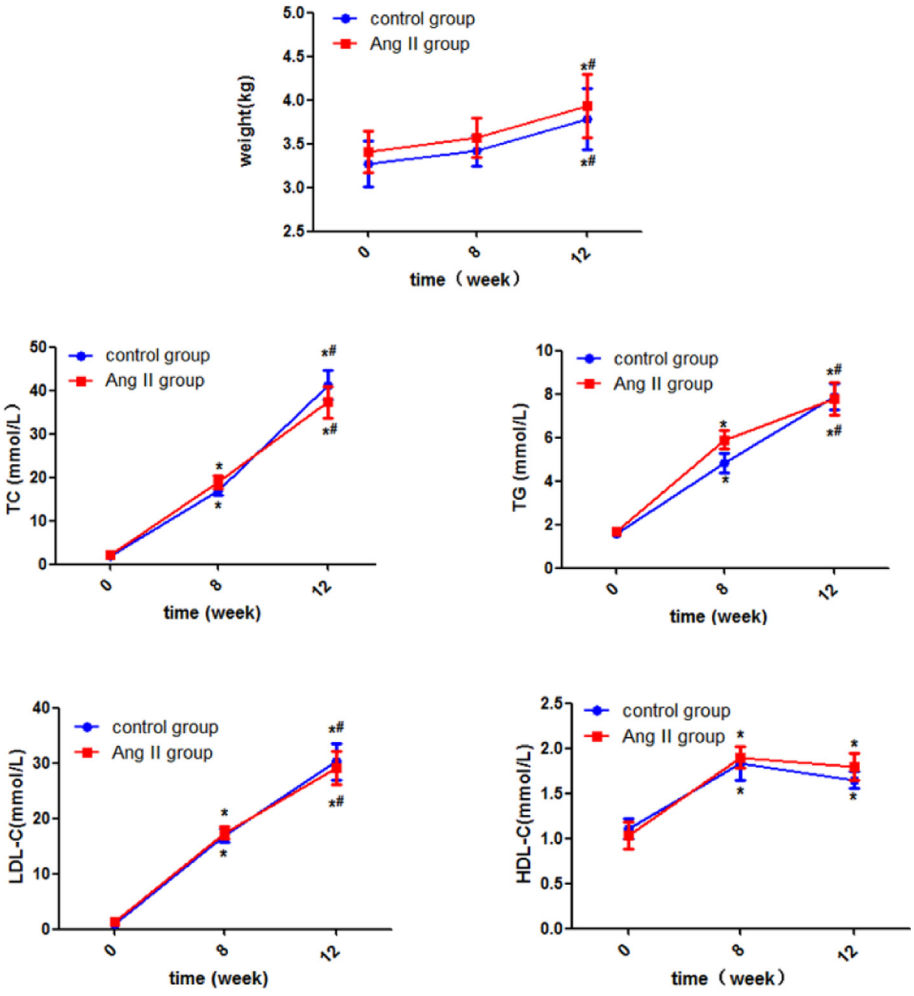

Fig. 1 Body weight and lipid profile of control and angiotensin II-treated rabbits. TC, total cholesterol; TG, triglycerides; LDL-C, low-density lipoprotein cholesterol and HDL-C, high-density lipoprotein cholesterol. Results are expressed as the mean ± S.E.M. "*" Each group compared with 0 weeks (baseline), $P < 0.01$. "#" Each group compared with 8 weeks, $P < 0.01$. Angiotensin II, Ang II.

Ang II–treated animals (Fig. 3). Fig. 3 also demonstrates that the expression of inflammatory marker PTX3 and neovascularization marker (CD31) were significantly higher in the Ang II group than in the control group.

3.3. Agreement between the MRI and the histopathological findings

Among the 126 carotid segments assessed histologically, 112 showed atherosclerosis ranging from AHA type I to VI. Forty-three segments displayed the early stages of atherosclerosis (AHA I–III), while 69 segments had advanced plaques (AHA IV–VI). Advanced atherosclerotic plaques were found more frequently in the Ang II group than the control group (68.1% vs 31.9%, $P < 0.001$). Based on the above results, the Cohen K value between the MR imaging and the AHA classification was 0.82 (0.73–0.91) ($P < 0.001$) (Table 1). Fig. 4 shows representative MR images and histopathology of a IV–V plaque (Fig. 4a at 12 weeks) and a VI plaque (Fig. 4c at 12 weeks). Fig. 4a at 12 weeks shows an MR image of an eccentric type IV–V plaque. The corresponding histological section confirmed the presence of an intact fibrous cap overlaying a lipid-core (Fig. 4b). The MR image of the type VI plaque shows a hyperintense signal in all sequences in the thickened vessel wall (Fig. 4c at 12 weeks). The corresponding histology (Fig. 4d) revealed the hyperintense site and confirmed the presence of intraplaque hemorrhage and abundant foam cells.

3.4. MRI measurements of plaque development in the Ang II and control groups

At 12 weeks, 90 of the total 112 axial vessel wall images contained plaque (AHA III–VI) according to the modified AHA criteria for MRI; 48 (53.3%) were in the Ang II group, and 42 (46.7%) were in the control group. At 8 weeks, no IPH were found in these two groups, and the plaque composition (LRNC area) and plaque burden (Max WT and VWA) were not significantly different between these two groups. In order to testify the accelerated effect of Ang II on atherosclerosis, the effect sizes of plaque composition and burden to detect plaque development during 8–12 weeks were calculated in these two groups (Table 2), which showed that significant changes were exhibited in VWA, max WT, and LRNC area in these

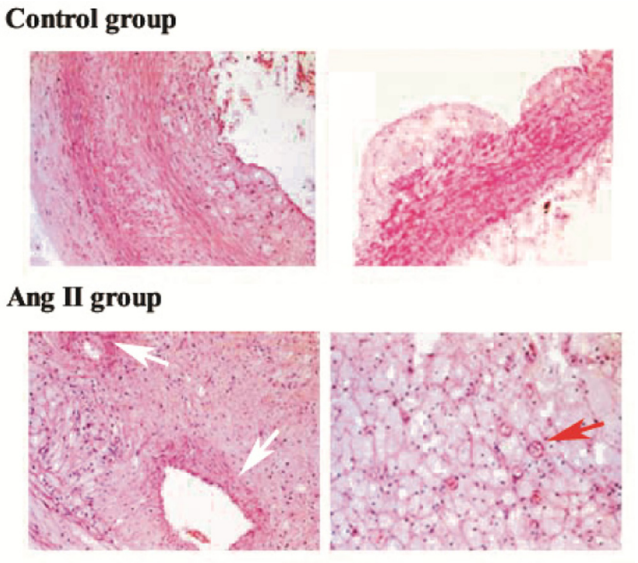

Fig. 2 The histopathologic features of angiotensin II–treated rabbits. (*Upper panel*) Plaque lesions from the control animals showed a thickened intima displaying smooth muscle cells in a matrix background in different regions of the vessel but with rare small intralesional vessels. (*Lower panel*) Plaque lesions in angiotensin II–treated rabbits display a more complex morphology characterized by large and more irregular intralesional vessels (*red arrow*) and the presence of intralesional hemorrhages (*white arrow*). Angiotensin II, Ang II.

two groups. In addition, the Ang II group has a greater effect size of the plaque parameters (VWA, max WT and LRNC area) than those of the control group. The morphologic changes of these two groups' LCCAs are illustrated in Fig. 4.

4. Discussion

The present study revealed the followings: (1) Ang II short-term administration prompts the vulnerability of carotid atheroma and creates more extensive plaque lesions by inducing intralesional hemorrhage and neovascularization as well as abundant inflammation in our rabbit atherosclerosis model; and (2) *in vivo* MRI is capable of accurately identifying and quantifying the major components of the carotid atherosclerotic plaques in the Ang II-treated rabbit model and can also monitor the development of carotid atherosclerotic plaques over time.

Plaque vulnerability is closely associated with the incidence of stroke and acute myocardial infarction. So, early and accurate detection of VPs is very important. In our study, Ang II was used to enhance plaque vulnerability, which induced neovascularization, IPHs, and inflammation. IPHs are considered prominent markers of plaque progression and instability, which are closely correlated with plaque disruption (Kolodgie et al., 2003). While, Valdeci et al. showed that besides Ang II-induced neovascularization, hemorrhage and inflammation, the plaque lesion is also accompanied by further expansive remodeling in apolipoprotein E–deficient mice. Ivan et al. demonstrated a close relationship between intimal inflammation and expansive remodeling in ligated arteries of apoE-KO mice (Ivan et al., 2002). Others have also claimed that expansively remodeled atherosclerotic vessels often give rise to more rupture-prone lesions (Schoenhagen et al., 2000). So our study, for the first time, explores the effect of Ang II on the combination of a high cholesterol diet and balloon injury in the LCCA, which is different from the ligation of the LCCA (aim to trigger the remodeling) in the study by Valdeci. Through these design differences, we included that Ang II-induced vulnerable features of plaques may be independent of the expansive remodeling process.

Ang II administration increases mechanical strain on the lesions by raising blood pressure, and Ang II–induced hypertension can accelerate the development of atherosclerosis in ApoE-deficient mice (Weiss et al., 2001). Ang II infusion into hyperlipidemic mice also augments lesion formation independent of elevation in blood pressure by eliciting a proinflammatory Th1-like phenotype or by increasing the angiogenic properties of the plaque (Mazzolai et al., 2004). Inflammatory mechanisms are known to play central roles in the pathogenesis and progression of atherosclerosis, plaque rupture and subsequent thrombosis and stroke. PTX3 is the prototypic member of the long pentraxin family that is produced at the site of inflammation in response to primary inflammatory stimuli by various cell types, including monocytes/macrophages, endothelial cells, vascular smooth muscle cells, fibroblasts, and adipocytes (Garlanda et al., 2005). PTX3 has been suggested as a marker of inflammatory activity and plaque instability (Matsuura et al., 2012). A number of studies have suggested PTX3 was associated with plaque vulnerability in the carotid and coronary arteries (Shindo et al., 2014; Hollan et al., 2013), Akihiro Shindo et al. have shown that serum PTX3 levels in both systemic and intracarotid samples before and after carotid artery stenting were higher in the vulnerable group than in the stable group. Neovessels within plaques characterized by fragility and high perfusion have also been considered to be an additional feature of VPs. These neovessels can increase the permeability of inflammatory cells, especially the presence of extensive macrophage accumulation (Chen et al., 2005; Lin et al., 2007). Multiple studies have emphasized a critical link between intravascularization and intralesional hemorrhage and instability by stimulating infiltrated inflammatory cells, which all play important roles in plaque progression and destabilization (Chen et al., 2005). In our study, plaque lesions in the Ang II group had extensive neovascularization; moreover, abundant macrophage cells as well as extensive staining for inflammation marker PTX3 were diffusedly distributed in the Ang II-treated vessel wall. So our data showed that the IPHs that occurred in the lesions in response to angiotensin II stimulation may be correlated with disrupted intralesional vessels and abundant inflammatory cell infusion. Our findings greatly substantiate the multipotent ability of Ang II to affect plaque vulnerability.

High-resolution MRI is a non-invasive technique to monitor the natural progression of atherosclerotic plaques not only including general features of a plaque but also some characteristics of a vulnerable plaque: a thin or ruptured fibrous cap, a large lipid-rich necrotic core, and intraplaque hemorrhage. With the rapid development of MRI in recent years, MRI studies on atherosclerosis in various vulnerable atherosclerotic animal models have been described. Our results showed that an MR vessel wall image can accurately identify and quantify the rapid carotid atherosclerotic progression in the Ang II-accelerated rabbit model over time. Ang II induced

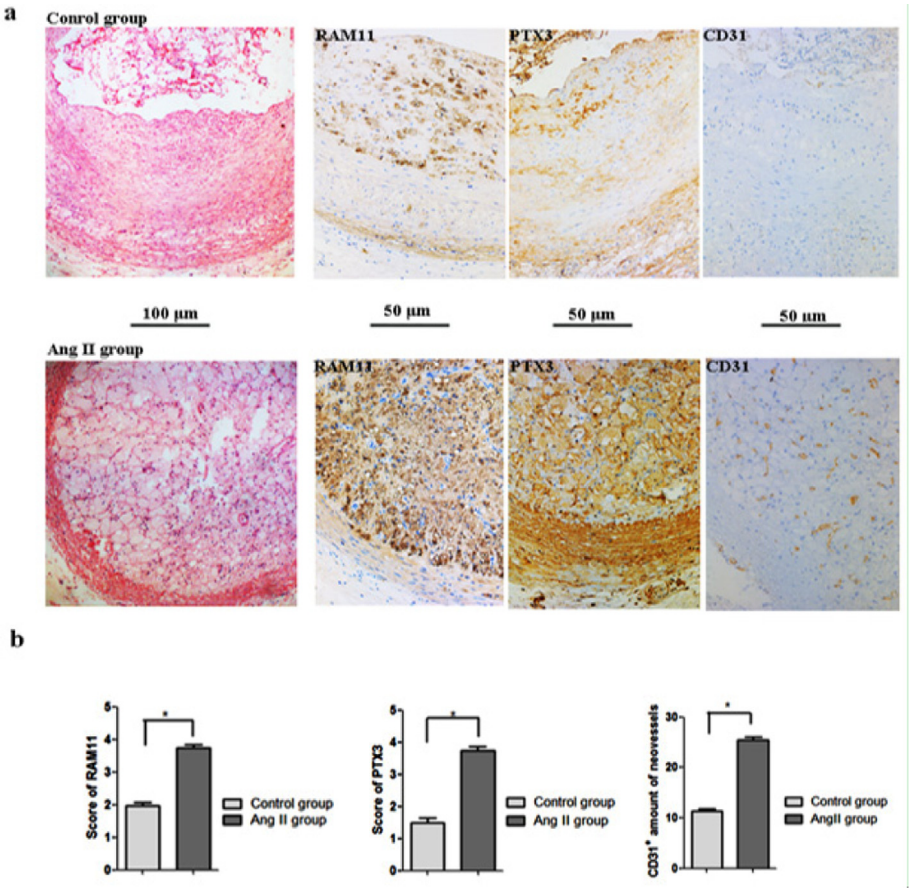

Fig. 3 Effect of angiotensin II on the expression of RAM11, PTX3 and CD31. Representative sections of the left common carotid arteries from the control (*Upper panel*) and angiotensin II–treated (*Lower panel*) rabbits after staining with hematoxylin and eosin and immunostaining for RAM11 and PTX3 expression and capillary density (a). The quantification of immunohistochemistry analysis of RAM11, PTX3, and CD31 staining of sections from artery tissues (b). $^{*}P < 0.05$. Angiotensin II, Ang II.

Table 1 The agreement between MRI and histopathologic findings via Cohen's Kappa test.

MRI type	Histology type					Kappa	*P*
	I–II	III	IV–V	VI	Total		
I–II	8	4	0	0	12	0.82(0.73–0.91)	<0.001
III	4	25	2	1	32		
IV–V	0	2	42	0	44		
VI	0	0	1	23	24		
Total	12	31	45	24	112		

Cohen's Kappa test.

more extensive lesions that enabled us to determine that there was a good correlation between MRI classifications and histopathological classifications in our rabbit models. Even these correlations have also been studied by others, prior authors either mainly focused on the relationship between the measurements of vessel wall thickness with MRI and histopathology (Wang et al., 2006) or have scarce plaques fulfill the criteria for advanced human atherosclerotic plaque. In addition, different from other MRI studies involving vulnerable atherosclerosis models, which were either long-term experiments with rare advanced lesions or involving a toxic-triggered thrombus that does not represent true plaque rupture (Ma et al., 2008, 2012), in our study, vulnerable plaques were induced by Ang II administration based on a classical high cholesterol-diet and endothelial injury. In particular, the intraplaque hemorrhage which is currently viewed as the driving force in plaque progression (Virmani et al., 2005) and regarded as prone to disruption (Kampschulte et al., 2004; Milei et al., 2003; Zhang, 2016), can be accurately and directly detected by MRI at 12 weeks even when plaque rupture, and an occlusive thrombus is not observed. Based on these observations, MRI analysis also showed that the Ang II accelerates atherosclerotic progression, which is indicated by a larger effective size of VWA, max WT, and LRNC area. Our study is the first to substantiate the proatherosclerotic effect of Ang II with MR vessel wall images.

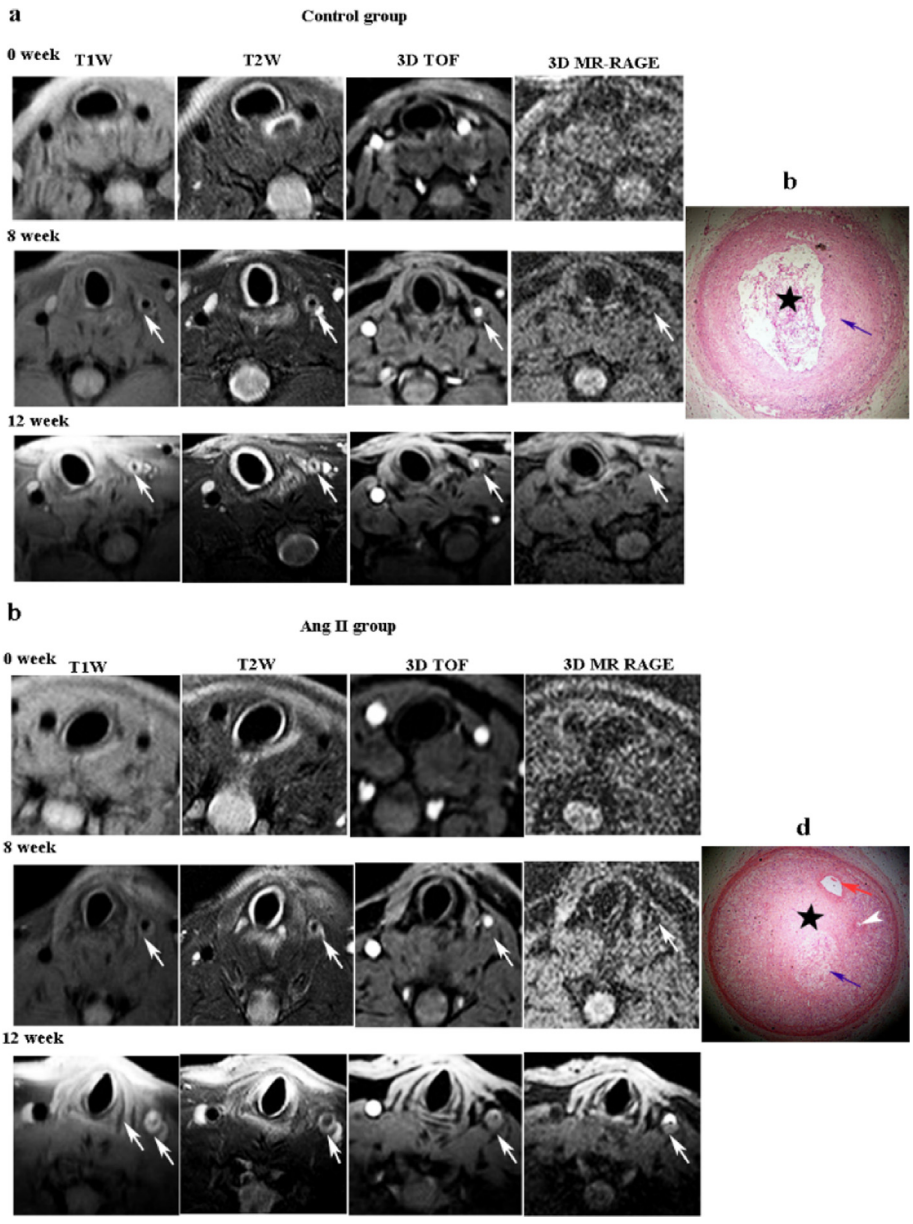

Fig. 4 MR images showed different development over time between the control group (a) and the angiotensin II-treated group (c), corresponding with histopathology (b and d). (a) In the control group, compared to the baseline MRI, the injured *LCCA* wall (*white arrow*) became thicker with hyperintense on T1WI and appeared isointense on T2WI in the 8th week. At the 12th week, the *LCCA* wall (*white arrow*) contained a plaque with hyperintensity on T1WI but appeared hypointense on T2WI and there were no hyperintensities in MP-RAGE (AHA IV–V). The histological section (b) corresponding to (a) showed plaques composed of foam cells (*blue arrow*) with a narrower lumen (*black star*, HE staining, ×40). (c) In the Ang II-treated group, the MRI showed that the injured *LCCA* wall (*white arrow*) contained a plaque with hyperintensity on T1WI and appeared hypointense on T2WI at the 8th week after 4 weeks of the Ang II treatment. The MRI demonstrated an advanced atherosclerotic plaque (*white arrow*) composed of IPH that appeared hyperintense on T1WI, TOF, MP-RAGE and appeared iso/hypointense on T2WI. The histological section (d) corresponding to (c) showed larger and more extensive plaques (AHA VI) composed of abundant foam cells (*blue arrow*), neovessels (*broad white arrow*) and IPH (*red arrow*) with a significantly narrower lumen (*blue star*, HE staining, ×40). Angiotensin II, Ang II; left common carotid artery, LCCA.

4.1. Limitations of this study

Our study has some limitations. First, the Ang II accelerated model of atherosclerosis resulted in a greater extent of atherosclerosis and a higher percentage of IPH but plaque CA, rupture and thrombosis were absent, perhaps because of short follow-up period in our study design. Another important issue involving our analysis of the consistency between MRI classifications and histopathological classifications, the MRI slice thickness (3 mm) is greater than that of the histological section (10 μm). The MR image represents a composite of 300 histology sections. To lessen this mismatch, we sectioned the tissue in 3.0-mm transverse slices corresponding to the MRI slice thickness and chose the histological sections for

Table 2 Comparison of the changes of LCCA over time of the Ang II group and control group.

Plaque parameters	8 weeks MRI	12 week MRI	Growth	*t*-value	Effective size
Control group (n = 42 slices)					
VWA (mm^2)	2.37 ± 0.74	4.85 ± 2.21	2.48 ± 2.26	7.12	1.09*
max WT (mm)	0.53 ± 0.23	1.10 ± 0.40	0.57 ± 0.42	8.59	1.32*
LRNC area (mm^2) (12 slices)	0.29 ± 0.35	2.77 ± 1.32	2.48 ± 1.43	6.18	1.78*
Ang II group (n = 48 slices)					
VWA (mm^2)	2.60 ± 4.07	8.45 ± 2.66	5.85 ± 4.94	8.19	1.18*
max WT (mm)	0.55 ± 0.14	1.29 ± 0.35	0.74 ± 0.41	12.56	1.81*
LRNC area (mm^2) (23 slices)	0.28 ± 0.46	3.27 ± 1.09	2.99 ± 1.20	11.68	2.43*

Effect sizes (t-value/n^{-2}) were compared using a t-test.
Data are means ± standard deviations.
VWA, vessel wall area; max wall thickness, max WT; lipid rich necrotic core, LRNC.
* $P < 0.05$

HE and IHC staining near the interval level. However, in some complex specimens containing lesions that may change significantly in size or composition from section to section, obtaining precise co-registration can be difficult. Also, due to the tissue degradation and dehydration, artifactual transformation of histological sections may occur. So, we performed HE and IHC staining as soon as possible after animals were sacrificed to reduce those possible influences.

In conclusion, as shown in this accelerated atherosclerotic rabbit model, our data further strengthen the effect of Ang II on promoting plaque vulnerability by inducing neovascularization, hemorrhage, and inflammation. Additionally, MR plaque imaging represents a useful modality for accurate assessment and follow-up evaluation of atherosclerotic progression that substantiated roles the roles of Ang II from the view of radiology.

Acknowledgements

This study was supported by National Natural Science Foundation of China (grants 81401374 and 81571630), Young Researcher Grant from Shanghai Municipal Commission of Health and Family Planning (20144Y0076) and Medical Engineering Cross Research Foundation of Shanghai Jiao Tong University (YG2016MS56).

References

Cai, J.M., Hatsukami, T.S., Ferguson, M.S., Small, R., Polissar, N.L., Yuan, C., 2002. Classification of human carotid atherosclerotic lesions with in vivo multicontrast magnetic resonance imaging. Circulation 106 (11), 1368–1373.

Chen, F., Eriksson, P., Kimura, T., Herzfeld, I., Valen, G., 2005. Apoptosis and angiogenesis are induced in the unstable coronary atherosclerotic plaque. Coron. Artery Dis. 16 (3), 191–197.

Cheng, C., Tempel, D., Van Haperen, R., Van der Baan, A., Grosveld, F., Daemen, M.J., Krams, R., De Crom, R., 2006. Atherosclerotic lesion size and vulnerability are determined by patterns of fluid shear stress. Circulation 113 (23), 2744–2753.

Curvo-Semedo, L., Lambregts, D.M., Maas, M., Thywissen, T., Mehsen, R.T., Lammering, G., Beets, G.L., Caseiro-Alves, F., Beets-Tan, R.G., 2011. Rectal cancer: assessment of complete response to preoperative combined radiation therapy with chemotherapy–conventional MR volumetry versus diffusion-weighted MR imaging. Radiology 260 (3), 734–743.

Da Cunha, V., Martin-McNulty, B., Vincelette, J., Choy, D.F., Li, W. W., Schroeder, M., Mahmoudi, M., Halks-Miller, M., Wilson, D. W., Vergona, R., Sullivan, M.E., Wang, Y.X., 2006. Angiotensin II induces histomorphologic features of unstable plaque in a murine model of accelerated atherosclerosis. J. Vasc. Surg. 44 (2), 364–371.

Daugherty, A., Manning, M.W., Cassis, L.A., 2000. Angiotensin II promotes atherosclerotic lesions and aneurysms in apolipoprotein E-deficient mice. J Clin Invest. 105 (11), 1605–1612.

Den Dekker, W.K., Tempel, D., Speelman, L., Huizingh, J., Ramos, A., Gijsen, F.J., Wentzel, J.J., Cheng, C., Duckers, H.J., 2014. Effect of shear stress alteration on atherosclerotic plaque vulnerability in cholesterol-fed rabbits. Vasc. Med. 19 (2), 94–102.

Den Hartog, A.W., Franken, R., De Witte, P., Radonic, T., Marquering, H.A., Van der Steen, W.E., Timmermans, J., Scholte, A.J., Van den Berg, M.P., Zwinderman, A.H., Mulder, B.J., Groenink, M., 2013. Aortic disease in patients with Marfan syndrome: aortic volume assessment for surveillance. Radiology 269 (2), 370–377.

Du, Q.L., Tang, W.S., Pan, L.A., 2016. Improved design of rotary controlled lift aircraft hydraulic mechanism. J. Mech. Eng. Res. Dev. 39 (1), 226–233.

Garlanda, C., Bottazzi, B., Bastone, A., Mantovani, A., 2005. Pentraxins at the crossroads between innate immunity, inflammation, matrix deposition, and female fertility. Annu. Rev. Immunol. 23, 337–366.

Hollan, I., Nebuloni, M., Bottazzi, B., Mikkelsen, K., Forre, O.T., Almdahl, S.M., Mantovani, A., Fagerland, M.W., Aukrust, P., Meroni, P.L., 2013. Pentraxin 3, a novel cardiovascular biomarker, is expressed in aortic specimens of patients with coronary artery disease with and without rheumatoid arthritis. Cardiovasc. Pathol. 22 (5), 324–331.

Ivan, E., Khatri, J.J., Johnson, C., Magid, R., Godin, D., Nandi, S., Lessner, S., Galis, Z.S., 2002. Expansive arterial remodeling is associated with increased neointimal macrophage foam cell content: the murine model of macrophage-rich carotid artery lesions. Circulation 105 (22), 2686–2691.

Kampschulte, A., Ferguson, M.S., Kerwin, W.S., Polissar, N.L., Chu, B., Saam, T., Hatsukami, T.S., Yuan, C., 2004. Differentiation of intraplaque versus juxtaluminal hemorrhage/thrombus in advanced human carotid atherosclerotic lesions by in vivo magnetic resonance imaging. Circulation 110 (20), 3239–3244.

Kohno, M., Ohmori, K., Nozaki, S., Mizushige, K., Yasunari, K., Kano, H., Minami, M., Yoshikawa, J., 2000. Effects of valsartan on angiotensin II-induced migration of human coronary artery smooth muscle cells. Hypertens. Res. 23 (6), 677–681.

Kolodgie, F.D., Gold, H.K., Burke, A.P., Fowler, D.R., Kruth, H.S., Weber, D.K., Farb, A., Guerrero, L.J., Hayase, M., Kutys, R., Narula, J., Finn, A.V., Virmani, R., 2003. Intraplaque hemorrhage and progression of coronary atheroma. N. Engl. J. Med. 349 (24), 2316–2325.

Laursen, J.B., Rajagopalan, S., Galis, Z., Tarpey, M., Freeman, B.A., Harrison, D.G., 1997. Role of superoxide in angiotensin II-induced but not catecholamine-induced hypertension. Circulation 95 (3), 588–593.

Lin, H.L., Xu, X.S., Lu, H.X., Zhang, L., Li, C.J., Tang, M.X., Sun, H.W., Liu, Y., Zhang, Y., 2007. Pathological mechanisms and dose dependency of erythrocyte-induced vulnerability of atherosclerotic plaques. J. Mol. Cell. Cardiol. 43 (3), 272–280.

Ma, Z.L., Teng, G.J., Chen, J., Zhang, H.Y., Cao, A.H., Ni, Y., 2008. A rabbit model of atherosclerosis at carotid artery: MRI visualization and histopathological characterization. Eur. Radiol. 18 (10), 2174–2181.

Ma, X., Zhao, Q., Zhao, L., Shang, J., Feng, T., Zeng, C., Zhang, Z., 2012. In vivo MR imaging of plaque disruption and thrombus formation in an atherosclerotic rabbit model. Int. J. Cardiovasc. Imaging 28 (3), 577–586.

Mao, W., Kong, J., Dai, J., Huang, Z.Q., Wang, D.Z., Ni, G.B., Chen, M.L., 2010. Evaluation of recombinant endostatin in the treatment of atherosclerotic plaques and neovascularization in rabbits. J. Zhejiang Univ. Sci. B 11 (8), 599–607.

Matsuura, Y., Hatakeyama, K., Imamura, T., Tsuruda, T., Shibata, Y., Kodama, T., Kitamura, K., Asada, Y., 2012. Different distribution of pentraxin 3 and C-reactive protein in coronary atherosclerotic plaques. J. Atheroscler. Thromb. 19 (9), 837–845.

Mazzolai, L., Duchosal, M.A., Korber, M., Bouzourene, K., Aubert, J.F., Hao, H., Vallet, V., Brunner, H.R., Nussberger, J., Gabbiani, G., Hayoz, D., 2004. Endogenous angiotensin II induces atherosclerotic plaque vulnerability and elicits a Th1 response in ApoE−/− mice. Hypertension 44 (3), 277–282.

Mervaala, E.M., Muller, D.N., Park, J.K., Schmidt, F., Lohn, M., Breu, V., Dragun, D., Ganten, D., Haller, H., Luft, F.C., 1999. Monocyte infiltration and adhesion molecules in a rat model of high human renin hypertension. Hypertension 33 (1 Pt 2), 389–395.

Milei, J., Parodi, J.C., Ferreira, M., Barrone, A., Grana, D.R., Matturri, L., 2003. Atherosclerotic plaque rupture and intraplaque hemorrhage do not correlate with symptoms in carotid artery stenosis. J. Vasc. Surg. 38 (6), 1241–1247.

Phinikaridou, A., Ruberg, F.L., Hallock, K.J., Qiao, Y., Hua, N., Viereck, J., Hamilton, J.A., 2010. In vivo detection of vulnerable atherosclerotic plaque by MRI in a rabbit model. Circ. Cardiovasc. Imaging 3 (3), 323–332.

Pueyo, M.E., Gonzalez, W., Nicoletti, A., Savoie, F., Arnal, J.F., Michel, J.B., 2000. Angiotensin II stimulates endothelial vascular cell adhesion molecule-1 via nuclear factor-kappaB activation induced by intracellular oxidative stress. Arterioscler. Thromb. Vasc. Biol. 20 (3), 645–651.

Qi, C., Deng, L., Li, D., Wu, W., Gong, L., Li, Y., Zhang, Q., Zhang, T., Zhang, C., Zhang, Y., 2015. Identifying vulnerable atherosclerotic plaque in rabbits using DMSA-USPIO enhanced magnetic resonance imaging to investigate the effect of atorvastatin. PLoS One 10 (5), e0125677.

Saam, T., Ferguson, M.S., Yarnykh, V.L., Takaya, N., Xu, D., Polissar, N.L., Hatsukami, T.S., Yuan, C., 2005. Quantitative evaluation of carotid plaque composition by in vivo MRI. Arterioscler. Thromb. Vasc. Biol. 25 (1), 234–239.

Schoenhagen, P., Ziada, K.M., Kapadia, S.R., Crowe, T.D., Nissen, S. E., Tuzcu, E.M., 2000. Extent and direction of arterial remodeling in stable versus unstable coronary syndromes: an intravascular ultrasound study. Circulation 101 (6), 598–603.

Shindo, A., Tanemura, H., Yata, K., Hamada, K., Shibata, M., Umeda, Y., Asakura, F., Toma, N., Sakaida, H., Fujisawa, T., Taki, W., Tomimoto, H., 2014. Inflammatory biomarkers in atherosclerosis: pentraxin 3 can become a novel marker of plaque vulnerability. PLoS One 9 (6), e100045.

Stary, H.C., Chandler, A.B., Dinsmore, R.E., Fuster, V., Glagov, S., Insull, W.J., Rosenfeld, M.E., Schwartz, C.J., Wagner, W.D., Wissler, R.W., 1995. A definition of advanced types of atherosclerotic lesions and a histological classification of atherosclerosis. A report from the Committee on Vascular Lesions of the Council on Arteriosclerosis, American Heart Association. Circulation 92 (5), 1355–1374.

Torzewski, M., Klouche, M., Hock, J., Messner, M., Dorweiler, B., Torzewski, J., Gabbert, H.E., Bhakdi, S., 1998. Immunohistochemical demonstration of enzymatically modified human LDL and its colocalization with the terminal complement complex in the early atherosclerotic lesion. Arterioscler. Thromb. Vasc. Biol. 18 (3), 369–378.

Virmani, R., Kolodgie, F.D., Burke, A.P., Finn, A.V., Gold, H.K., Tulenko, T.N., Wrenn, S.P., Narula, J., 2005. Atherosclerotic plaque progression and vulnerability to rupture: angiogenesis as a source of intraplaque hemorrhage. Arterioscler. Thromb. Vasc. Biol. 25 (10), 2054–2061.

Wang, Y.X., Kuribayashi, H., Wagberg, M., Holmes, A.P., Tessier, J. J., Waterton, J.C., 2006. Gradient echo MRI characterization of development of atherosclerosis in the abdominal aorta in Watanabe Heritable Hyperlipidemic rabbits. Cardiovasc. Intervent. Radiol. 29 (4), 605–612.

Weiss, D., Kools, J.J., Taylor, W.R., 2001. Angiotensin II-induced hypertension accelerates the development of atherosclerosis in apoE-deficient mice. Circulation 103 (3), 448–454.

Zhang, H.B., 2016. Element modeling and dynamic property parameters analysis of self-anchored suspension bridge. J. Mech. Eng. Res. Dev. 39 (1), 39–45.

Zhang, Y., Yao, J., Huan, L., Lian, J., Bao, C., Li, Y., Ge, C., Li, J., Yao, M., Liang, L., He, X., 2015. GNAI3 inhibits tumor cell migration and invasion and is post-transcriptionally regulated by miR-222 in hepatocellular carcinoma. Cancer Lett. 356 (2 Pt B), 978–984.

Zhao, H., Zhao, X., Liu, X., Cao, Y., Hippe, D.S., Sun, J., Li, F., Xu, J., Yuan, C., 2013. Association of carotid atherosclerotic plaque features with acute ischemic stroke: a magnetic resonance imaging study. Eur. J. Radiol. 82 (9), e465–470.